JOURNAL OF PROPULSION AND POWER
Vol. 26, No. 1, January–February 2010

Ion Thruster Grid Design Using an Evolutionary Algorithm

Cody C. Farnell* and John D. Williams†
Colorado State University, Fort Collins, Colorado 80523

DOI: 10.2514/1.44358

An evolutionary algorithm was used to optimize the geometry and accelerator grid voltage of an ion thruster grid set with regard to maximizing impulse per unit area, essentially equivalent to maximizing propellant throughput capability per unit area. Grid operating conditions, including a net accelerating voltage of 1800 V and current density of 4.0 mA/cm^2, corresponded to high-power operation of NASA's evolutionary xenon thruster. The evolutionary-algorithm-derived grid set had a predicted lifetime nearly twice that of the NASA's evolutionary xenon thruster grid set, primarily the result of a lower accelerator grid voltage magnitude.

Nomenclature

A_g	=	aperture grid area
$c1$, $c2$	=	child chromosomes
$\bar{c}$	=	mean neutral speed
d_c	=	intermediate recombination constant
d_m	=	mutation range
d_s, d_a	=	screen or accel grid hole diameter
$E_{\max}$	=	electric field
e	=	elementary charge
F	=	aperture thrust
f	=	fitness value
f_p	=	perveance fraction
ft	=	thrust factor
J_b, J_{be}	=	beamlet current
J^{++}/J^{+}	=	double-to-single current ratio
j, j_e	=	downstream current density
j_p	=	upstream current density
k	=	mutation precision
L	=	predicted grid lifetime
l_{cc}	=	aperture center-to-center spacing
l_e	=	effective ion acceleration length
l_g	=	grid spacing
m_i	=	ion mass
$\dot{m}_{\text{Aeq}}$	=	propellant flow rate
P	=	perveance
$P_{\max}$	=	maximum perveance
p_c, p_m	=	recombination or mutation probability
$p1$, $p2$	=	parent chromosomes
R	=	net-to-total voltage ratio
R_m	=	mutation fraction of variable range
r_c, r_m	=	random numbers
t_s, t_a	=	screen or accel grid thickness
V_D	=	discharge voltage
V_m	=	margin against electron backstreaming
V_N	=	net accelerating voltage
V_s, V_a	=	screen or accel grid potential
V_T	=	total accelerating voltage
W_0	=	neutral transmission probability
ε_0	=	permittivity of free space
η_u	=	propellant utilization efficiency
ϕ	=	ion transparency
ϕ_s, ϕ_a	=	screen or accel grid open-area fraction

Received 16 March 2009; revision received 1 September 2009; accepted for publication 8 September 2009.

*Postdoctoral Researcher, Department of Mechanical Engineering, 1374 Campus Delivery. Member AIAA.

†Assistant Professor, Department of Mechanical Engineering, 1374 Campus Delivery. Senior Member AIAA.

I. Introduction

ONE component of an electric propulsion ion thruster that may be life-limiting is the ion optics assembly, or grids, used to accelerate ions from the discharge chamber to produce thrust [1,2]. Charge-exchange ions erode both the accelerator (or accel) grid hole barrel and downstream face, which can lead to electron backstreaming and/or accel grid structural failure. Ion thrusters designed for future deep space missions require increasingly robust optics. For instance, as of June 2008, an engineering model, NASA's evolutionary xenon thruster (NEXT), had accumulated over 16,550 h of operation and processed 337 kg of xenon propellant during a long-duration test (LDT) designed to validate the thruster's mission throughput requirement of 300 kg [3].

Present ion optics designs for deep space thrusters, such as those of NEXT and NSTAR (NASA's solar technology application readiness), consist of two grids, the geometry of which is depicted in Fig. 1 [3,4]. The relationship between individual grid parameters and grid performance and lifetime is complex and difficult to test experimentally, due to the large number of combinations and expected lifetime capabilities. Accordingly, simulation codes, such as the ffx code [5,6] and others [7–11], have been developed to predict grid performance and lifetime. The ffx code has been validated against experimental data from both the NEXT and NSTAR ion thrusters [5,12].

Consider the problem of maximizing the impulse per unit area provided by an aperture, given in Eq. (1). This is the thrust F provided by an aperture multiplied by the operation time L, normalized to its area A_g. The downstream current density $j = J_b/A_g$, the propellant (xenon, which determines m_i), the double-to-single current ratio J_b^{++}/J_b^{+}, and the net accelerating voltage V_N were chosen as independent constant variables. The dependent variables, which could be calculated using the ffx code, were the grid lifetime L and thrust factor ft.

The quantity to be maximized, or the fitness value f, given in Eq. (2), was chosen as the predicted operation lifetime multiplied by the thrust factor, which takes into account beamlet divergence multiplied by the grid transparency to ions (ϕ) taken to a power. A high ion transparency minimizes discharge chamber losses [13]:

$$\frac{F \cdot L}{A_g} = \frac{J_b}{A_g} L \frac{m_i}{e} \left[\left(1 + \frac{\sqrt{2}}{2} \frac{J_b^{++}}{J_b^{+}} \right) \Big/ \left(1 + \frac{J_b^{++}}{J_b^{+}} \right) \right] ft \sqrt{\frac{2eV_N}{m_i}} \quad (1)$$

$$f = L \cdot ft \cdot \phi^4 \quad (2)$$

An evolutionary algorithm, one of many global optimization techniques, was applied to this problem. Six unknown variables were

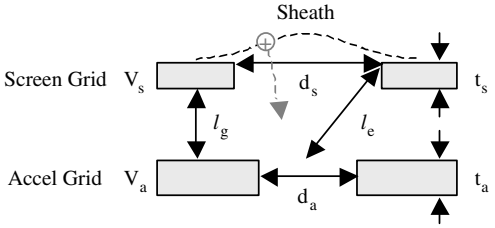

Fig. 1 Two-grid ion optics geometry.

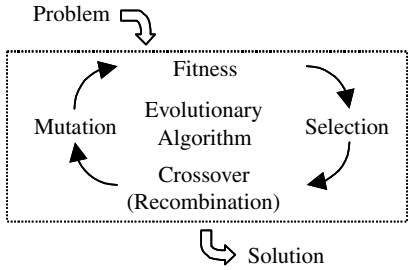

Fig. 2 Outline of an evolutionary algorithm.

used to maximize the fitness value: screen grid thickness t_s, screen grid hole diameter d_s, grid spacing l_g, accel grid thickness t_a, accel grid hole diameter d_a, and accel grid voltage V_a. The evaluation function was a simulation, the ffx code, which provided lifetime, thrust factor, and ion transparency predictions given a set of input parameters.

II. Evolutionary Algorithm

Genetic algorithms and evolution strategies are two subcategories of evolutionary algorithms, both of which generally mimic biological evolution to seek problem solutions [14]. The general overview of an evolutionary algorithm is presented in Fig. 2. The algorithm works with a population of solutions called chromosomes. Each chromosome codes for a set of values for the unknown variables of the problem.

Initially, on generation zero, the chromosomes were generated randomly. The algorithm used the ffx code to evaluate the chromosomes and assign them fitness values. Selection, crossover/recombination, and mutation were then used to form the next (it is hoped, improved) generation. Genetic algorithms tend to use binary value encoding and large chromosome populations and to favor crossover over mutation; evolution strategies tend to use real-value encoding and smaller populations and to favor mutation over recombination [14,15]. The algorithm in this work, using a 100-chromosome population and real-value encoding, would be considered closer to an evolution strategy than a genetic algorithm. An evolutionary algorithm was appropriate for this problem, as it could use the ffx code to evaluate many sets of input grid geometries and operating conditions in parallel.

The use of a genetic algorithm for electric propulsion thruster design was first demonstrated by Nakayama and Wilbur in 2001 [16]. In that work, Nakayama and Wilbur developed a Thruster Performance Evaluation Code (TPEC), which was used in a genetic algorithm to optimize a discharge chamber design. The results of the algorithm were in good agreement with experimental data. In following work, Nakayama and Wilbur [17] used an algorithm with the igx ion optics code for grid design at high specific impulse ($\sim$10 kV) . The fitness value used there maximized the thrust factor multiplied by a beam current ratio taken to a power to expand differences between the chromosomes. The algorithm was run at several fixed beamlet currents, resulting in maximized thrust and minimized accel grid charge-exchange ion impingement current. Additionally, Nakayama and Wilbur's [17] fitness values were set to zero if electron backstreaming was not avoided. Five genes were used per chromosome, which coded for screen grid thickness, grid gap, accel grid potential, accel grid hole diameter, and accel grid thickness. The screen grid potential (10 kV) and the screen grid hole diameter (7 mm) were held constant. In those cases, the optimization was considered complete on or before the 80th generation, in which 100 chromosomes were used per generation. In both of the studies by Nakayama and Wilbur [16,17], genetic algorithms were successfully used with simulation codes as the method of fitness-value evaluation.

Table 1 reports the methods used in the evolutionary algorithm applied to the present problem. To ensure that the spread of fitness values was neither too large nor too small, linear rank-based fitness assignment was performed using a selective pressure of 2.0 [18]. This method reassigned the chromosome fitness values from 2.0 (best) to 0.0 (worst) following evaluation using the ffx code. Elitism was used, with the best chromosome from a generation copied directly to the next without alteration. The remaining population was filled through recombination and mutation operations. After choosing two chromosomes using roulette-wheel selection [18], recombination was applied at a rate of 75%, and mutation of individual parameters was applied at a rate of 25%. The probability of selection in the roulette-wheel method is proportional to an individual's fitness-value magnitude. The methods of intermediate recombination and mutation for real-value chromosome encoding are described in [18,19].

For illustration, consider parent chromosomes $p1$ and $p2$ that were chosen to create child chromosomes $c1$ and $c2$. In Table 2, recombination was applied if $r_c \leq p_c$, where $r_c = [0, 1]$ was a uniform random number and p_c was the recombination rate. If recombination occurred, the value of each variable v_i (t_s, d_s, etc.) in $c1$ and $c2$ became a random combination of the corresponding variable values in $p1$ and $p2$. For variable v_i, a uniform random number r_i was chosen that determined the linear combination factor a_i. The constant d_c was set to 0.25 so that the child variable domain was statistically as large as the parent variable domain [19]. Mutation occurred if $r_m \leq p_m$, where a different $r_m = [0, 1]$ was chosen for each child chromosome variable and p_m was the mutation rate. The mutation rate was set to $1.5/n$, where n was the number of variables (six), so that, on average, 1.5 variables per child chromosome were mutated. Here, d_m was the mutation range, which was a fraction R_m of each variable's acceptable domain, and k was the mutation precision. With this scheme, small mutations occurred more often than large mutations.

The algorithm determined fitness values in parallel, using nine ffx programs to evaluate 11 chromosomes on each generation (one chromosome was directly transferred between generations). Each chromosome took 10 to 15 min to evaluate, which involved solving

Table 1 Guidelines for the evolutionary algorithm

Feature	Value/method
Population	100 chromosomes
Encoding	Real value
Scaling	Rank selection. Selective pressure is 2.0
Selection	Roulette wheel
Elitism	Yes, best chromosome
Recombination	Intermediate recombination. Rate $p_c = 75\%$
Mutation	$R_m = 0.5$, $k = 8$, and rate $p_m = 1.5/6 = 25\%$

Table 2 Recombination and mutation scheme

Recombination[a]	
If $r_c \leq p_c$	If $r_c > p_c$
Recombination occurs	No recombination
$v_{c1} = v_{p1}a_1 + v_{p2}(1 - a_1)$	$v_{c1} = v_{p1}$
$v_{c2} = v_{p1}a_2 + v_{p2}(1 - a_2)$	$v_{c2} = v_{p2}$
Mutation[b]	
If $r_m \leq p_m$	If $r_m > p_m$
Mutation occurs	No mutation
$v'_{ci} = v_{ci} + sd_m a_m$	$v'_{ci} = v_{ci}$

[a] $a_i = r_i + d_c(2r_i - 1)$ for $r_i = [0, 1]$, $a_i = [-d_c, 1 + d_c]$, and $d_c = 0.25$.
[b] $s = -1$ or $+1$, $d_m = R_m(v_{\max} - v_{\min})$, $R_m = 0.5$, $a_m = 2^{-u \cdot k}$, $u = [0, 1]$, and $k = 8$.

for the beamlet shape and calculating charge-exchange ion erosion rates.

III. Fitness Value

The evaluation function (in this case, the ffx code) provided lifetime, thrust factor, ion transparency, and electron backstreaming margin data to the algorithm based upon the constant input conditions and the independent variables of each chromosome.

A. Constant Input Conditions

Two throttle points of the NEXT LDT were used to define the constant operating conditions. Operation at a net voltage of 1800 V and beam current of 3.52 A is expected to lead to structural failure of the accel grid, due to groove wear-through, and the greatest amount of crossover ion impingement is expected at a net voltage of 1800 V and beam current of 1.2 A, due to operation at low perveance [20].

For a beam current of 3.52 A and a flatness parameter of 0.84 [3], the centerline current density was near 4.0 $\mathrm{mA/cm^2}$. The double-to-single current ratio and net accelerating voltage were set to 8% and 1800 V, respectively [3]. A discharge voltage V_D of 25 V set the screen grid voltage V_s to 1775 V. The screen grid physical open-area fraction ϕ_s was specified to be 66.7% (typical). Finally, the discharge propellant utilization efficiency η_u was set to 89%. The fitness value was evaluated at these conditions.

Because ion thrusters normally obtain power from solar arrays, it is necessary to have throttling capability as the available power varies with distance from the sun [4]. For the NEXT LDT 1.2 A beam current, 1800 V condition, the current density near the edge of the thruster (j_e) is near 0.5 $\mathrm{mA/cm^2}$ [3], and it is here that crossover ion impingement is most likely. Acceptable solutions were required to operate at this current density with no crossover impingement. If crossover was observed, the fitness value was set to zero.

B. Independent Variables

Each chromosome coded directly for the six unknown variables: screen grid thickness t_s, screen grid hole diameter d_s, grid spacing l_g, accel grid thickness t_a, accel grid hole diameter d_a, and accel grid voltage V_a.

C. Dependent Variables

Certain values, dependent upon the input conditions and chromosome variable values, were set at run time: aperture center-to-center spacing l_{cc}, through the specified physical screen grid transparency ϕ_s,

$$l_{\mathrm{cc}} = \sqrt{\frac{\pi}{2\sqrt{3}}\frac{d_s^2}{\phi_s}}$$

and beamlet currents J_b and J_{be}, through the specified current densities j and j_e and center-to-center spacing l_{cc},

$$J_b = A_g j = \frac{\sqrt{3}}{2} l_{\mathrm{cc}}^2 j$$

$$J_{be} = A_g j_e = \frac{\sqrt{3}}{2} l_{\mathrm{cc}}^2 j_e$$

D. Fitness-Value Evaluation

There are several possible end-of-life mechanisms for an ion thruster. Two possibilities related to accel grid erosion are structural failure, due mainly to pit and/or groove wear-through, and the onset of electron backstreaming, due mainly to hole barrel enlargement and grid thinning. Electron backstreaming was the end-of-life mechanism for the NSTAR extended-life-test (ELT) [21], whereas groove wear-through is thought to be the most likely end-of-life mechanism for the NEXT LDT [20]. Accordingly, the end-of-life mechanism depends on the grid geometry and operation conditions.

The evolutionary algorithm needed to quickly evaluate many potential solutions. As a result, lifetime predictions were calculated from beginning-of-life erosion rates. To encompass both structural and electron backstreaming failure mechanisms, the end-of-life of the accel grid was taken to be the time at which 40% of the accel grid mass was worn away. Several full-length simulations using variations of the NEXT grid geometry showed that this was the point at which the onset of electron backstreaming was predicted. Full-length simulations could be used to determine grid lifetimes and identify the end-of-life mechanisms; however, these simulations would increase the algorithm runtime significantly and were not feasible. Although full-length lifetime simulations were not used, beginning-of-life predictions were observed to be within ±8% of postalgorithm full-length predictions.

In addition to assigning fitness values based on lifetime, thrust factor, and ion transparency, limits were placed on acceptable solutions' margins against electron backstreaming (V_m) and unionized propellant transmission probability (W_0). A greater-than-40-V margin against electron backstreaming was required to guarantee that electron backstreaming was mitigated over the entire expected lifetime. This requirement was seen to be sufficient from full-length lifetime simulation of the algorithm solution.

To independently optimize grid geometry, similar conditions within the discharge chamber must exist with respect to neutral density, discharge voltage, and double-to-single ion current ratio. The neutral density n_0 within the discharge chamber is given in Eq. (3), where j is the current density, $\bar{c}$ is the mean neutral speed, η_u is the propellant utilization efficiency, $\dot{m}_{\mathrm{Aeq}}$ is the propellant flow rate in amps-equivalent, J_b^{++}/J_b^{+} is the double-to-single current ratio, and W_0 is the overall neutral transmission probability. To obtain an equivalent neutral density, current density, propellant utilization efficiency, and double-to-single current ratio, the neutral transmission probability must be equivalent among grid sets. The overall transmission probability is calculated from the physical open-area fractions and transmission probabilities (Clausing factors [22]) of the screen and accel grids, as indicated in Eq. (4) [23]. Acceptable algorithm solutions were required to have a neutral transmission probability less than 0.132 (that of NEXT):

$$\begin{aligned} n_0 &= \frac{4j}{e\bar{c}W_0}\left(\frac{1-\eta_u}{\eta_u}\right)\frac{1+\frac{1}{2}(J_b^{++}/J_b^{+})}{1+(J_b^{++}/J_b^{+})} \\ \bar{c} &= \sqrt{\frac{8kT}{\pi m_i}} \\ \eta_u &= \frac{J_b}{\dot{m}_{\mathrm{Aeq}}}\frac{1+\frac{1}{2}(J_b^{++}/J_b^{+})}{1+(J_b^{++}/J_b^{+})} \end{aligned} \tag{3}$$

$$\begin{aligned} \frac{1}{W_0} &= \frac{1}{\phi_s W_s} + \frac{1}{\phi_a W_a} \\ \phi_i &= \frac{\pi}{2\sqrt{3}}\left(\frac{d_i}{l_{\mathrm{cc}}}\right)^2 \quad i = s, a \\ W_i &= f\left(\frac{t_i}{d_i}\right) \quad i = s, a \end{aligned} \tag{4}$$

(see [22]).

E. Variable Ranges

Perveance fraction f_p was used to help determine minimum and maximum allowed variable values that encompassed the expected results. Perveance P (in $\mathrm{A/V^{3/2}}$) is a measure of the current density j_p passing between two surfaces according to a specified potential difference and separation. The perveance fraction, as applied to ion optics, is given in Eq. (5). A perveance fraction of unity indicates that the maximum possible current density is being extracted for the given total accelerating voltage V_T and effective ion acceleration length l_e.

Table 3 Allowed variable ranges

Variable	Lower limit	Upper limit
t_s	0.25	$(t_s/d_s)_{\text{typ}} d_{s\max}$
d_s	1.0	$d_{s\max}$
l_g	$((V_N/R_{0.9}) - V_d)/E_{\max}$	$(l_g/d_s)_{\text{typ}} d_{s\max}$
t_a	0.25	$l_{e\max}$
d_a	1.0	$d_{s\max}$
V_a	$V_N(1 - (1/R_{\min}))$	$V_N(1 - (1/R_{\max}))$

The downstream current density j is lower than the upstream current density j_p by the factor of the ion transparency ϕ:

$$f_p = \frac{j_p}{P_{\max}} \frac{l_e^2}{V_T^{3/2}}, \qquad P_{\max} = \frac{4\varepsilon_0}{9}\sqrt{\frac{2e}{m_i}}$$
$$l_e = \sqrt{(l_g + t_s)^2 + \frac{1}{4}d_s^2}, \qquad V_T = V_N - V_a, \qquad j = j_p\phi \tag{5}$$

The upper limits for t_s, d_s, and l_g were determined using the maximum ion acceleration length $l_{e\max}$ at a perveance fraction of unity [Eq. (6)]. The R ratio V_N/V_T was expected to be near 0.9, and the ion transparency was expected to be near the physical screen grid open-area fraction. Typical l_g/d_s and t_s/d_s ratios (from NEXT) were used to determine $d_{s\max}$ from $l_{e\max}$ [Eq. (7)]. In turn, $l_{g\max}$ and $t_{s\max}$ were determined from $d_{s\max}$ using the ratios. Minimum grid thicknesses and hole diameters were chosen to be 0.25 and 1.0 mm, respectively. A thermal/structural analysis (for example, that of [24]) was not performed to determine minimum values and was beyond the scope of this work. For the accel grid voltage, the R ratio was allowed to vary between 0.85 and 0.95. A maximum electric field of 3 kV/mm was imposed to determine the minimum grid spacing. The lower and upper variable limits, listed in Table 3, encompassed the NEXT and NSTAR grid geometries and operating conditions, with the exception of the minimum grid spacing, where the operating electric fields of the NEXT and NSTAR thrusters are greater than 3 kV/mm:

$$l_{e\max} = \sqrt{\frac{P_{\max}(V_N/0.9)^{3/2}}{j/\phi_s}} \tag{6}$$

$$l_{e\max}^2 = d_{s\max}^2 \left\{ \left[\left(\frac{l_g}{d_s}\right)_{\text{typ}} + \left(\frac{t_s}{d_s}\right)_{\text{typ}} \right]^2 + \frac{1}{4} \right\} \tag{7}$$

IV. Results

The variable values of the best chromosome in the population are shown in Fig. 3 through generation 50. Convergence, in which the optimum chromosome values were not changing for many generations, was implied by generation 100.

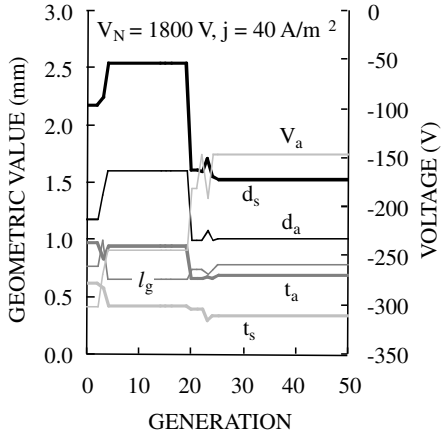

Fig. 3 History of the most fit chromosome in each generation.

Table 4 Evolutionary algorithm and NEXT grid performance

Parameter	EA solution	NEXT
	Beginning of life	
Beamlet (ion density)		
$L/L_{\text{NEXT40\%ML}}$	1.78	1 (unity)
ft	0.99	0.97
ϕ, %	72	93
V_a, V	−146	−210
V_m, V	45	39
	Lifetime simulations	
$L/L_{\text{NEXT40\%ML}}$	1.92	0.95

Table 5 Evolutionary algorithm solution and NASA's evolutionary NEXT grid geometry

Parameter	EA solution	NEXT
l_{cc}/d_s	1.17	1.16
t_s/d_s	0.17	0.20
d_s/d_s	Unity	Unity
l_g/d_s	0.27	0.23
t_a/d_s	0.43	0.40
d_a/d_s	0.65	0.64
W_0	0.13	0.13

Table 4 compares the evolutionary algorithm grid to the NEXT grid operating at a current density of 4.0 mA/cm^2. According to beginning-of-life erosion rates, the evolutionary algorithm (EA) grid was predicted to last 78% longer than the NEXT grid, mainly due to its lower accel grid voltage. Full-length lifetime simulations showed a slight increase in the predicted lifetime for the EA grid and a slight decrease for the NEXT grid, both within 8% of the beginning-of-life predictions.

Table 5 compares the grid geometry found using the evolutionary algorithm to the NEXT grid geometry, with selected values normalized to the respective grid's screen grid hole diameter d_s. The algorithm solution had a slightly thinner screen grid and thicker accel grid compared to NEXT. Because of a larger (operating) grid gap, the EA solution operated at a slightly higher perveance fraction than the NEXT grid (at the same current density).

V. Discussion

For nearly equivalent ion transparencies, 70–75%, and thrust factors, 0.98–0.99, the main factor in the fitness value of this study was found to be the accel grid lifetime. To maximize lifetime, it was desirable for the algorithm to decrease neutral density, which lowered charge-exchange ion production, and increase accel grid mass.

For constant propellant utilization efficiency, the algorithm was observed to decrease neutral density by increasing the neutral transmission probability W_0 [Eq. (3)]. If the transmission probability was not limited to a maximum value, the algorithm solution went to a large d_a/d_s ratio near 1. This was not immediately intuitive, as alternatively decreasing the accel diameter would increase accel grid mass. However, allowing the neutral density within the discharge chamber to decrease would likely cause changes in the double-to-single current ratio and discharge voltage among others, making direct comparisons between grid sets difficult. The inclusion of a model to examine discharge chamber–grid interactions, such as

those of [25], [26], or [27], was beyond the scope of this work but would represent a future algorithm improvement.

To increase accel grid mass, the accel grid thickness was maximized under the constraint of operating with no accel grid ion impingement at the low 0.5 $\mathrm{mA/cm^2}$ current density. If the grid was not required to operate at this low current density (i.e., with no throttling requirement imposed), the solution went to a very thick accel grid with t_a/d_s near 1. A second reason for maximizing accel grid thickness was to minimize the accel grid voltage magnitude, which minimized charge-exchange ion impingement energy and sputter erosion rate.

The only independent variable constrained by its allowed variable range was the accel grid hole diameter, which was nearly minimized to 1.0 mm. The screen grid hole diameter, screen grid thickness, and grid spacing were similarly small, which indicated that the grid preferred to operate at a low perveance fraction: in this case, 0.27 at 4.0 $\mathrm{mA/cm^2}$. Operating at a low perveance fraction had the effect of funneling a large fraction of the charge-exchange ions created in the intragrid region through the accel grid hole and out of the grid set rather than into the accel grid. A small screen grid thickness also helped to increase ion transparency.

VI. Conclusions

An evolutionary algorithm was used in conjunction with the ffx ion optics code to design a grid set toward the goal of maximizing impulse per unit area. The algorithm-derived grid set had a predicted lifetime nearly twice that of the NEXT grid set at a current density of 4.0 $\mathrm{mA/cm^2}$ and beam current of 1800 V. The EA and NEXT grid sets had similar normalized geometrical ratios. The evolutionary algorithm favored grid sets that minimized neutral density, maximized accel grid mass, and minimized the magnitude of the accel grid voltage.

References

[1] Brophy, J. R., and Polk, J. E., "Ion Engine Service Life Validation by Analysis and Testing," 32nd AIAA/ASME/SAE/ASEE Joint Propulsion Conference and Exhibit, Lake Buena Vista, FL, AIAA Paper 1996-2715, July 1996.

[2] Soulas, G. C., "Improving the Total Impulse Capability of the NSTAR Ion Thruster With Thick-Accelerator-Grid Ion Optics," 27th International Electric Propulsion Conference, Pasadena, CA, Paper IEPC 2001-081, Oct. 2001.

[3] Herman, D. A., Soulas, G. C., and Patterson, M. J., "NEXT Long-Duration Test Plume and Wear Characteristics after 16,550 h of Operation and 337 kg of Xenon Processed," 44th AIAA/ASME/SAE/ASEE Joint Propulsion Conference and Exhibit, Hartford, CT, AIAA Paper 2008-4919, July 2008.

[4] Brophy, J. R., "NASA's Deep Space 1 Ion Engine," *Review of Scientific Instruments*, Vol. 73, No. 2, Feb. 2002, Paper 1432470. doi:10.1063/1.1432470

[5] Farnell, C. C., "Performance and Lifetime Simulation of Ion Thruster Optics," Ph.D. Dissertation, Dept. of Mechanical Engineering, Colorado State Univ., Fort Collins, CO, 2007.

[6] Farnell, C. C., Williams, J. D., and Wilbur, P. J., "Numerical Simulation of Ion Thruster Optics," 28th International Electric Propulsion Conference, International Electric Propulsion Conference Paper 03-073, Toulouse, France, March 2003.

[7] Nakayama, Y., and Wilbur, P. J., "Numerical Simulation of Ion Beam Optics for Many-Grid Systems," 37th AIAA/ASME/SAE/ASEE Joint Propulsion Conference and Exhibit, Salt Lake City, UT, AIAA Paper 2001-3782, July 2001.

[8] Emhoff, J. W., and Boyd, I. D., "Modeling of Total Thruster Performance for NASA's Evolutionary Xenon Thruster Ion Optics," *Journal of Propulsion and Power*, Vol. 22, No. 4, 2006, pp. 741–748. doi:10.2514/1.18975

[9] Wang, J., Cao, Y., Kafafy, R., Martinez, R., and Williams, J., "Numerical and Experimental Investigations of Cross-Over Ion Impingement for Sub-Scale Ion Optics," 43rd AIAA/ASME/SAE/ASEE Joint Propulsion Conference and Exhibit, Cincinnati, OH, AIAA Paper 2007-5244, July 2007.

[10] Wirz, R. E., Anderson, J. R., Katz, I., and Goebel, D. M., "Time-Dependent Erosion of Ion Optics," 44th AIAA/ASME/SAE/ASEE Joint Propulsion Conference and Exhibit, Hartford, CT, AIAA Paper 2008-4529, July 2008.

[11] Malone, S. P., "Investigation of NEXT Ion Optics Erosion Processes Using Computational Modeling," *Joint Army Navy NASA Air Force Conference*, Monterey, CA, Paper 2005-0356, Dec. 2005.

[12] Farnell, C. C., Williams, J. D., and Wilbur, P. J., "NEXT Ion Optics Simulation via ffx," 39th AIAA/ASME/SAE/ASEE Joint Propulsion Conference, AIAA Paper 2003-4869, Huntsville, AL, July 2003.

[13] Goebel, D. M., and Katz, I., *Fundamentals of Electric Propulsion: Ion and Hall Thrusters*, Wiley, Hoboken, NJ, 2008, pp. 96, 196.

[14] Back, T., and Schwefel, H., "An Overview of Evolutionary Algorithms for Parameter Optimization," *Evolutionary Computation*, Vol. 1, No. 1, 1993, pp. 1–23. doi:10.1162/evco.1993.1.1.1

[15] Whitley, D., "An Overview of Evolutionary Algorithms: Practical Issues and Common Pitfalls," *Information and Software Technology*, Vol. 43, No. 14, 2001, pp. 817–831. doi:10.1016/S0950-5849(01)00188-4

[16] Nakayama, Y., and Wilbur, P. J., "The Feasibility of a Genetic-Algorithm-Based Ion Thruster Design Code," 37th AIAA/ASME/SAE/ASEE Joint Propulsion Conference and Exhibit, AIAA Paper 2001-3786, Salt Lake City, UT, July 2001.

[17] Nakayama, Y., and Wilbur, P. J., "Numerical Simulation of High Specific Impulse Thruster Optics," *27th International Electric Propulsion Conference*, International Electric Propulsion Conference Paper 2001-99, Pasadena, CA, Oct. 2001.

[18] Pohlheim, H., "Evolutionary Algorithms: Overview, Methods and Operators," Dec. 2006, http://www.geatbx.com/download/GEATbx_Intro_Algorithmen_v38.pdf [retrieved 20 Jan. 2009].

[19] Muhlenbein, H., and Schlierkamp-Voosen, D., "Predictive Models for the Breeder Genetic Algorithm 1: Continuous Parameter Optimization," *Evolutionary Computation*, Vol. 1, No. 1, 1993, pp. 25–49. doi:10.1162/evco.1993.1.1.25

[20] Van Noord, J. L., and Herman, D. A., "Application of the NEXT Ion Thruster Lifetime Assessment to Thruster Throttling," 44th AIAA/ASME/SAE/ASEE Joint Propulsion Conference and Exhibit, AIAA Paper 2008-4526, Hartford, CT, July 2008.

[21] Sengupta, A., Brophy, J. R., Anderson, J. R., Garner, C., de Groh, K., Karniotis, T., and Banks, B., "An Overview of the Results from the 30,000 hr Life Test of Deep Space 1 Flight Spare Ion Engine," 40th AIAA/ASME/SAE/ASEE Joint Propulsion Conference and Exhibit, AIAA Paper 2004-3608, Fort Lauderdale, FL, July 2004.

[22] Clausing, P., "The Flow of Highly Rarefied Gases Through Tubes of Arbitrary Length," *Journal of Vacuum Science and Technology*, Vol. 8, No. 5, 1971, pp. 636–646. doi:10.1116/1.1316379

[23] Yu-Guo, F., "The Problem of the Approximation Calculation for Molecular Conductance," *Vacuum*, Vol. 31, No. 7, 1981, pp. 319–324. doi:10.1016/S0042-207X(81)80504-0

[24] Soulas, G. C., "Calculation of Thermally-Induced Displacements in Spherically Domed Ion Engine Grids," 29th International Electric Propulsion Conference, International Electric Propulsion Conference Paper 2005-248, Princeton, NJ, 2005.

[25] Goebel, D., Wirz, R., and Katz, I., "Analytical Ion Thruster Discharge Performance Model," *Journal of Propulsion and Power*, Vol. 23, No. 5, 2007, pp. 1055–1067. doi:10.2514/1.26404

[26] Brophy, J. R., "Ion Thruster Performance Model," NASA CR-174810; also Ph.D. Dissertation, Dept. of Mechanical Engineering, Colorado State Univ., Fort Collins, CO, 1984.

[27] Mahalingam, S., "Particle Based Plasma Simulation for an Ion Engine Discharge Chamber," Ph.D. Dissertation, Dept. of Mechanical and Materials Engineering, Wright State Univ., Dayton, OH, 2007.

J. Blandino
Associate Editor